J. Cent. South Univ. (2012)19: 3435–3443
DOI: 10.1007/s11771-012-1426-2

Springer

Space luminous environment adaptability of missile-borne star sensor

ZHAO Shu-fang(赵述芳)[1], WANG Hong-tao(王洪涛)[2], WANG Yu(王渝)[1] , JI Cai-yan(纪彩彦)[3]

1. School of Automation, Beijing Institute of Technology, Beijing 100081, China;
2. Beijing Institute of Control and Electronic Technology, Beijing 100038, China;
3. Tianjin Medical Instrumentation Inspection Centre of SDA, Tianjin 300191, China

Abstract: To solve the problem of stray interference to star point target identification while a star sensor imaging to the sky, a study on space luminous environment adaptability of missile-borne star sensor was carried out. By Plank blackbody radiation law and some astronomic knowledge, irradiancies of the stray at the star sensor working height were estimated. By relative astrophysical and mathematics knowledge, included angles between the star sensor optical axis point and the stray at any moment were calculated. The calculation correctness was verified with the star map software of Stellarium. By combining the upper analysis with the baffle suppression effect, a real-time model for space luminous environment of missile-borne star sensor was proposed. By signal-noise rate (SNR) criterion, the adaptability of missile-borne star sensor to space luminous environment was studied. As an example, a certain type of star sensor was considered when imaging to the starry sky on June 22, 2011 (the Summer Solstice) and September 20, 2011 (August 23 of the lunar year, last quarter moon) in Beijing. The space luminous environment and the adaptability to it were simulated and analyzed at the star sensor working height. In each period of time, the stray suppression of the baffle is analyzed by comparing the calculated included angle between the star sensor optical axis point and the stray with the shielded provided by system index. When the included angle is larger than the shielded angle and less than 90°, the stray is restrained by the baffle. The stray effect on star point target identification is analyzed by comparing the irradiancy of 6 magnitude star with that of the stray on star sensor sensitization surface. When the irradiancy of 6 magnitude star is 5 times more than that of the stray, there is no effect on the star point target identification. The simulation results are identical with the actual situation. The space luminous environment of the missile-borne star sensor can be estimated real-timely by this model. The adaptability of the star sensor to space luminous environment can be analyzed conveniently. A basis for determining the relative star sensor indexes, the navigation star chosen strategy and the missile launch window can be provided.

Key words: missile-borne star sensor; space luminous environment; stray; irradiancy; baffle; real-time model

1 Introduction

Missile-borne star sensor was a key device in INS/CNS. As an integrated navigation system, INS/CNS was made up of the missile-borne star sensor and the inertial navigation system. The requirement for initial alignment was allowed to be loosed up. The emission point localization orientation error, initial alignment error, and gyroscope drift error could be corrected by the star sensor observing the navigation star during flight. The guidance accuracy, the mobile launch ability and the quick response capability of ballistic missile especially long-range strategic missile could be improved [1−2].

Missile-borne star sensor works in the middle stage of a flight with 100−200 km above the earth. It is in the exoatmospheric and vacuum environment. When it images the starry sky, the stray of the sunlight, the moonlight and the earth-atmosphere radiation (EAR) might enter into the field of view (FOV). The image background would be enhanced by the stray. The star point target might be submerged and the navigation star identification might be failed. A spaceborne test of star sensor developed by Mitsubishi Company was conducted on SERVIS-1 satellite launched in 2003. Since the stray enters into the FOV, the edge part of star images takes on whiteness [3]. A spaceborne camera of certain satellite launched by China reaches the performance requirement in design stage. For being lack of strict theoretical analysis and calculation for stray extinction design in development stage, the stray restraining measures were not considered carefully. As a result, the background stray brightness was several hundred times higher than that of the expected imaged 5 magnitude star. The target image was fully submerged by the stray. A two-stage baffle was then added. Though the imaged star

Received date: 2011–11–11; **Accept date:** 2012–05–17
Corresponding author: ZHAO Shu-fang PhD; Tel: +86–13401111369; E-mail: zsf158@163.com

magnitude was up to 3.5, the performance requirement was not satisfied [4]. Therefore, space luminous environment was a key premise to be applied successfully for star sensor.

The characteristics of star sensor itself were concerned by researcher all the time. Many progresses had been made on star point recognition algorithm [5], measurement accuracy [6] and calibration algorithm [7]. But little research was carried out on space luminous environment adaptability of star sensor. As a research blank in the field of star sensor, few relative references could be found. Fortunately, some theories and methods in other fields (satellite observation, on-orbit spacecraft application, etc) were available.

In Refs. [8−10], the sun radiation model was given when the sun was regarded as an absolute blackbody. In Ref. [11], the theoretical value of the sun irradiancy in visible wavelength range in exoatmosphere was modified based on the basic radiation theory. The position vector relationship of the sun and the satellite in geocentric equatorial coordinate system at any moment was expounded. For the similarity of research objects, an idea for this work could be obtained by Ref. [11]. Then the sun irradiancy in the wavelength range of star sensor at the working height could be estimated. The coordinate of the sun in geocentric equatorial coordinate system could be calculated.

According to Refs. [12−13], the astronomical parameters for calculating the moon position were provided by BROWN in 1919. The ecliptic longitude and ecliptic latitude of the moon at any moment could be calculated by them. A basis for research could be provided by the references. The apparent right ascension and apparent declination of the moon could be obtained by the transformation formulas from the ecliptic plane to the equator plane. Furthermore, the coordinate in geocentric equatorial coordinate system could be obtained.

A concrete description of the EAR was given in Ref. [14], which meant all kinds of radiation released to the space by the earth-atmosphere system. The effect of the EAR on astronomical observation loads and star sensors operating in the low earth orbit (LEO) was pointed out in Ref. [15]. The EAR environment analysis of on-orbit spacecrafts was carried out in Ref. [16], and a simplified EAR distribution calculating model for spacecrafts was established. The earth was regarded as a diffuse body in Ref. [17]. Lambertian Law was followed by the reflection to the sun. The earth and its atmosphere system reflectivity to the sunlight could be taken as the earth mean reflectivity. A reference was provided by the literatures. For simplifying, the approximation method in Ref. [17] could be adopted to estimate the EAR irradiancy at the star sensor working height.

With the theories and methods all above, a thorough research on space luminous environment adaptability of missile-borne star sensor would be carried out in this work.

2 Model for space luminous environment

2.1 Theoretical analysis of stray irradiancy

2.1.1 Theoretical analysis of sun irradiancy

According to Planck blackbody radiation law, the monochrome irradiancy of blackbody radiation (W/m^3) could be expressed as

$$M_\lambda = (c_1 / \lambda^5)(\exp(c_2 / \lambda T_0) - 1)^{-1} \tag{1}$$

where λ is the wavelength (m); T_0 is the blackbody temperature (K); c_1=3.742×10^{-16} W·m^2; c_2=1.4388×10^{-2} m·K.

In the wavelength range from λ_1 to λ_2, the irradiancy M (W/m^2) of blackbody could be integrated from Eq. (1) as

$$M = c_1 \int_{\lambda_2}^{\lambda_1} \lambda^{-5} \{\exp[c_2 / (\lambda T)] - 1\}^{-1} \mathrm{d}\lambda \tag{2}$$

If the radius of a spherical blackbody is R, the total radiant flux in the wavelength range from λ_1 to λ_2 could be expressed as

$$\Phi = 4\pi R^2 M \tag{3}$$

The sun could be considered as a blackbody with the absolute temperature of T_0=5 900 K and the radius of R_s=6.959 9×10^8 m [8]. The monochrome irradiancy $M(\lambda, T_0)$ of the sun, the irradiancy M in the wavelength range from λ_1 to λ_2, the total radiant flux Φ could be figured out by Eq. (1), Eq. (2) and Eq. (3), respectively.

When the total radiant flux emitted by the sun was supposed to be uniform in all space directions, the luminous intensity of the sun in the wavelength range from λ_1 to λ_2 was

$$I_S = \Phi / 4\pi = R_S^2 M \tag{4}$$

If the energy attenuation in space transmission process caused by reflection and scattering of other celestial bodies or cosmic dust was neglected, the sun irradiancy (W/m^2) at the star sensor in the wavelength range from λ_1 to λ_2 could be expressed as follows according to the inverse distance square law [9−10]:

$$E_s = I_s / R_{ss}^2 = R_s^2 c_1 R_{ss}^{-2} \int_{\lambda_1}^{\lambda_2} \lambda^{-5} \left\{\exp[c_2 / (\lambda T) - 1]\right\}^{-1} \mathrm{d}\lambda \tag{5}$$

where R_{ss} is the distance from the sun to the star sensor. In one year, the distance from the sun to the earth was changed mainly caused by the earth orbit eccentricity. The correction coefficient K_0 of the distance for different time and different seasons could be expressed as [11]

$$K_0=\left(R_{se}/R_{ss}\right)^2=1.000\ 11+0.034\ 221\cos\varphi+ 0.001\ 28\sin\varphi+0.000\ 719\cos 2\varphi-0.000\ 077\sin 2\varphi \quad (6)$$

where R_{se} is the annual average distance from the sun to the earth, R_{se} = 1.4968×10^{11} m; φ is the day angle, which is the corresponding angle on 2π circumference of an arbitrary day in a year, $\varphi=2\pi(d_n-1)/365$, d_n is Julian days, which is the accumulation days from January 1st to an arbitrary day.

The change of the sun irradiancy at star sensor at any moment could be obtained through Eq. (5). In the spectral range (400 nm−1000 nm), the irradiancy curve of the sun at star sensor working height at noon in one year is shown in Fig. 1. It could be known from Fig. 1 that the maximum irradiancy was 918.1 W/m^2 and the minimum irradiancy was 857.3 W/m^2.

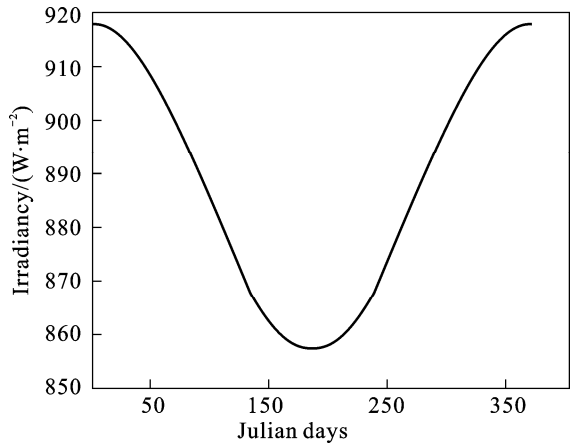

Fig. 1 Sun irradiancy at star sensor working height in star sensor spectral range

2.1.2 Theoretical analysis of moon irradiancy

Generally, the signal lightness of space point target was equivalent to star magnitude in astronomy. Since the illuminance produced by a zero apparent magnitude star in exoatmosphere was defined as $E_V(0)=2.65\times10^{-6}$ lx, the illuminance (lx) produced by a star with apparent star magnitude m in exoatmosphere was

$$E_{Vm}=E_{V0}\times10^{-m/2.5}=2.65\times10^{-(6+m/2.5)} \quad (7)$$

When the apparent star magnitude m and the color temperature T of a star body were known, the monochromatic irradiancy (W/m^3) of this star body in exoatmosphere could be expressed as [18]

$$E_\lambda(m,T)=M_S(\lambda,T)\frac{E_{Vm}}{M_V(T)} \quad (8)$$

where $M_S(\lambda, T)$ is the monochrome irradiancy (W/m^3) of blackbody radiation, which could be calculated by Eq. (1). $M_V(T)=683\int_0^\infty M_S(\lambda,T)V(\lambda)\mathrm{d}\lambda$, where $V(\lambda)$ is the luminosity function.

The radiation of the moon by itself could be approximate to the radiation of an absolute blackbody of 400 K, with the peak wavelength of 7.24 μm. In the spectral range of star sensor (400 nm−1 000 nm), the visible light given out by the moon was mostly the reflected sunlight. When other planets of the solar system were the brightest, the magnitudes of them were at least 8 times higher than that of the moon. So the effect by them could be neglected [19]. The brightness of the moon varied not only with the angular distance between the sun and the moon, but also with the distance between the earth and the moon. The brightness was the highest at full moon, with the apparent star magnitude of −12.2 and the color temperature of 5 900 K. Referencing the value of $V(\lambda)$, the integration of Eq. (8) in the visible range (380 nm−760 nm) could be turned into a summation operation with an interval of 10 nm by Matlab. Thus the value $E_{Vm}/M_V(T)$ could be obtained. The moon monochromatic irradiancy in exoatmosphere could be obtained by Eq. (8). In the spectral range of star sensor, the distribution of the monochromatic irradiancy was shown in Fig. 2. The total irradiancy of the moon in this band at full moon could be obtained as 0.001 4 W/m^2. Therefore, when the included angle between the star sensor axis point and the moonlight was less than 90°, it could be considered approximatively that the moon irradiancy at the star sensor was 0.001 4 W/m^2.

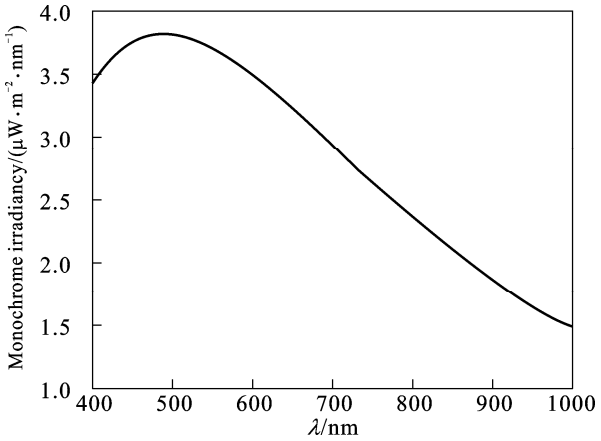

Fig. 2 Moon monochrome irradiancy curve in exoatmosphere

2.1.3 Theoretical analysis of EAR irradiancy

The EAR was the radiation released by the earth-atmosphere system (a space system whose lower limit was the earth surface and upper limit was the aeropause) to the interstellar space [14]. It was a serious interference factor in spacecrafts detecting faint objects and remote sensing applications, especially for astronomical observation loads and star sensors operating in LEO [15].

The earth itself could not shine, but it could be shiny by reflecting sunlight. After the sunlight enters into

the earth atmosphere, one part was reflected back into the space, and the other was scattered, reflected and absorbed by the atmosphere and the surface material. For the existence of thermal equilibrium, the earth would radiate out part of the absorbed energy with long wave. The earth could be regarded as a blackbody of 300 K, with the peak wavelength of 10 μm [16]. Because the peak wavelength (less than 2 μm) was rather small, the earth radiation could be neglected for the star sensor. It was a complicated process for the atmosphere and the surface material to scatter and reflect to the sun. For further analysis, it could be assumed that the earth was a diffuse reflector. The reflection to the sun followed Lambertian Law and was uniform everywhere. The reflectance spectrum is similar to the spectrum of the sun. The earth and its atmosphere system reflectivity to the sunlight generally was taken as the earth mean reflectivity, which was ρ=0.35 [17]. Then the EAR irradiancy at star sensor working height could be expressed as

$$E_e = \rho E_s = 0.35E_s \tag{9}$$

where E_s is the sun irradiancy at the star sensor working height and could be calculated by Eq. (5).

2.2 Position coordinates of stray

2.2.1 Unit position coordinate of star sensor optical axis point

When a star sensor imaged the starry sky, the missile would adjust the body attitude to let the star sensor optical axis align at a certain navigation star. Right ascension α_{star} and declination δ_{star} of the navigation star could be known in advance. Then the coordinate of the star sensor in geocentric equatorial coordinate system could be expressed as

$$\begin{cases} X_{star} = \cos\alpha_{star} \cdot \cos\delta_{star} \\ Y_{star} = \sin\alpha_{star} \cdot \cos\delta_{star} \\ Z_{star} = \sin\delta_{star} \end{cases} \tag{10}$$

For convenience, it was resumed that the star sensor optical axis was vertical and pointed to the sky when imaging. If the geographic longitude, geographic altitude and the above sea level were τ, ϕ and H, respectively, the local sidereal time could be expressed as [11]

$$T_{cz} = T_{gl} + \tau \tag{11}$$

The Greenwich local sidereal time $T_{gl} = T_{gl0} + T_{ms} \times 1.002\ 737\ 9 \times 2\pi$, where T_{gl0} is the Greenwich sidereal time of zero universal time of January 1st in the observed year, with the unit of radian, T_{ms} is the mean sun days (from the observation moment to 0:00 of January 1st), $T_{gl0} = 1.731\ 334\ 499 + 628.331\ 951C + 0.000\ 006\ 756C^2$, and C is the Julian century number calculated from the day of January 0.5, 1 900. C= (Julian day of a certain moment − Julian day of January 0.5, 1 900)/36 525. Then, the coordinate of star sensor in geocentric equatorial coordinate system could be expressed as

$$\begin{cases} X_{star} = G_1 \cdot \cos\phi \cdot \cos T_{cz} \\ Y_{star} = G_1 \cdot \cos\phi \cdot \sin T_{cz} \\ Z_{star} = G_2 \cdot \sin\phi \end{cases} \tag{12}$$

where

$$G_1 = a_e\sqrt{1-\left(2f-f^2\right)\cdot\sin^2\phi} + H;$$

$$G_2 = a_e\left(1-f\right)^2\sqrt{1-\left(2f-f^2\right)\cdot\sin^2\phi} + H;$$

a_e is the earth mean equatorial radius; f = 1/298.26 is the earth oblateness.

2.2.2 Included angle between star sensor optical axis point and sunlight

The motion of the sun relative to the earth followed Kepler Law. Its apparent motion was made up of the time changes of apparent right ascension α_s and apparent declination δ_s. Kepler equation was as follows [19−21]:

$$E - e\cdot\sin E = M \tag{13}$$

where E is the eccentric anomaly of the sun; M is the mean anomaly of the sun, $M = \omega(t - t_0)$; ω is the mean angular velocity of the sun to the earth, ω= 0.985 61×2π/360; t is the instantaneous moment of the sun (in Julian day); t_0 is the moment of January 3.02, 1950 (in Julian day); e=0.016 708 62–0.000 042 04 C–0.000 000 124 C^2, is the orbital eccentricity of the sun to the earth. With the series expansion of elliptical motion, the true anomaly could be obtained:

$$\begin{aligned} \theta = M &+ e\left(2 - e^2/4 + 5e^4/96\right)\cdot\sin M + \\ &e^2\left(5/4 - 11e^2/24\right)\cdot\sin 2M + \\ &e^3\left(13/12 - 43e^2/64\right)\cdot\sin 3M + \\ &103e^4\cdot\sin 4M/96 + 1097e^5\cdot\sin 5M/960 \end{aligned} \tag{14}$$

According to the definition of ecliptic, the ecliptic latitude of the sun is β_s=0. It was known that the sun passed by the pericenter on January 3.02, 1950. The corresponding ecliptic longitude was ω_0 = 282°4′.5. Then the ecliptic longitude of the moment t was

$$\lambda_s = \omega_0 + \theta \tag{15}$$

By

$$\begin{cases} \sin\delta_s = \sin\varepsilon\cdot\sin\lambda_s \\ \tan\delta_s = \cos\varepsilon\cdot\tan\lambda_s \end{cases}$$

it could be obtained that

$$\begin{cases}\alpha_s = \lambda_s + q\cdot\sin(2\lambda_s) + q^2\cdot\sin(4\lambda_s) + q^3\cdot\sin(2\lambda_s)/3 \\ \delta_s = \arcsin(\sin\varepsilon\cdot\sin\lambda_s)\end{cases} \tag{16}$$

where ε is the mean obliquity of the sun; $\varepsilon = 23°27'8''.26 - 46''.845C - 0''.0059C^2 + 0''.00181C^3$; $|q|<1$, $q=(\cos\varepsilon-1)/(\cos\varepsilon+1)$.

According to the definitions of right ascension and declination, the unit position coordinate of the sun in geocentric equatorial coordinate system could be expressed as

$$\begin{cases}X_s = \cos\alpha_s\cdot\cos\delta_s \\ Y_s = \sin\alpha_s\cdot\cos\delta_s \\ Z_s = \sin\delta_s\end{cases} \tag{17}$$

The included angle between the star sensor optical axis point and the sunlight could be expressed as

$$\theta_{ss} = \arccos\frac{X_{star}\cdot X_s + Y_{star}\cdot Y_s + Z_{star}\cdot Z_s}{\sqrt{\left(X_{star}^2 + Y_{star}^2 + Z_{star}^2\right)\left(X_s^2 + Y_s^2 + Z_s^2\right)}} \tag{18}$$

2.2.3 Included angle between star sensor optical axis point and moonlight

In 1919, the astronomical parameters (s, p, N) for calculating the moon position were provided by Brown [15]. s was the mean ecliptic longitude of the moon, with an angular velocity of 0.549 016 5(°)/h. p was the mean ecliptic longitude of the moon at perigee, with an angular velocity of 0.004 641 8(°)/h. N was the mean ecliptic longitude of the moon at ascending node, with an angular velocity of 0.000 002 0(°)/h. The computational formulae were shown as follows [12−13]:

$$s = 270.696\,88 - 481\,267.890\,57C - 0.001\,98C^2 + 0.000\,002C^3 \tag{19}$$

$$p = 334.329\,56 - 4\,069.340\,3C - 0.010\,32C^2 + 0.000\,01C^3 \tag{20}$$

$$N = 259.183\,28 - 1\,934.142\,01C - 0.002\,08C^2 + 0.000\,02C^3 \tag{21}$$

where C is the Julian century numbers from the day of January 0.5, 1900.

When the above-mentioned astronomical parameters were known, the ecliptic longitude λ_m and the ecliptic latitude β_m of the moon at any moment could be expressed as

$$\lambda_m = s + 0.109\,760\sin(s-p) + 0.022\,236\sin(2-2h+p) + 0.011\,490\sin(2s-2h) + 0.003\,728\sin(2s-2p) \tag{22}$$

$$\beta_m = 0.089\,504\sin(s+N) + 0.00\,489\,7\sin(2s-p+N) + 0.004\,847\sin(p-N) + 0.003\,024\sin(s-2h+N) \tag{23}$$

where h is the mean ecliptic longitude of the sun. h = 279.696 68 + 36 000.768 92 C + 0.000 30 C^2.

According to the transformation formulae from the ecliptic plane coordinate to the equatorial plane coordinate, the apparent right ascension α_m and apparent declination δ_m could be expressed as

$$\begin{cases}\tan\alpha_m = \left(\sin\lambda_m\cdot\cos\varepsilon - \tan\beta_m\cdot\sin\varepsilon\right)/\cos\lambda_m \\ \sin\delta_m = \sin\beta_m\cdot\cos\varepsilon + \cos\beta_m\cdot\sin\varepsilon\cdot\sin\lambda_m\end{cases} \tag{24}$$

where ε is the mean obliquity of the sun. $\varepsilon = 23°27'8''.26 - 46''.845C - 0''.0059C^2 + 0''.00181C^3$.

The unit position coordinate of the moon in geocentric equatorial coordinate system could be expressed as

$$\begin{cases}X_m = \cos\alpha_m\cdot\cos\delta_m \\ Y_m = \sin\alpha_m\cdot\cos\delta_m \\ Z_m = \sin\delta_m\end{cases} \tag{25}$$

The included angle between the star sensor optical axis point and the moonlight could be expressed as

$$\theta_{sm} = \arccos\frac{X_{star}\cdot X_m + Y_{star}\cdot Y_m + Z_{star}\cdot Z_m}{\sqrt{\left(X_{star}^2 + Y_{star}^2 + Z_{star}^2\right)\left(X_m^2 + Y_m^2 + Z_m^2\right)}} \tag{26}$$

2.2.4 Included angle between star sensor optical axis point and EAR

When a star sensor imaged the starry sky, the height was only about 100−200 km which was far less than the earth radius. So the EAR could not be regarded as a pointolite and should be treated as an extended source. When the included angle between the ligature (from the star sensor to the geocenter) and the star sensor optical axis was less than θ_H, as shown in Fig. 3, the EAR would enter into the star sensor FOV. The included angle between the star sensor optical axis point and the EAR could be considered as 0° at this time. θ_H could be calculated by

$$\theta_H = \arcsin\left(\frac{R_e}{R_e + H}\right) \tag{27}$$

where H is the height of the star sensor imaging to the starry sky; R_e is the mean radius of the earth, R_e = 6 371 km. When H is supposed to be 150 km, it could be known from Eq. (27) that θ_H = 77.7°.

When a star sensor imaged to a certain navigation star, the included angle between the star sensor optical axis point and the EAR could be expressed as

$$\theta_{sc}=90°-77.790°+\delta_{star}=12.3°+\delta_{star} \tag{28}$$

where δ_{star} is the declination value of a certain navigation star. If the star sensor optical axis is vertical and pointed to the sky, δ_{star} could be regard as 90°.

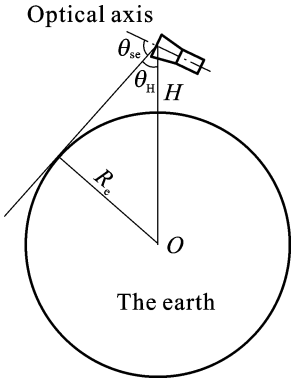

Fig. 3 Schematic diagram of EAR and star sensor optical axis

2.3 A real-time model for space luminous environment of missile-borne star sensor

For imaging to the starry sky, a star sensor should install a baffle (Fig. 4) to restrain interference of the sunlight, the moonlight and the EAR. Through the discussions all above, when a star sensor imaged, the real-time model for space luminous environment at the optical lenses could be expressed as

$$E_{stray} = E_{ss} + E_{se} + E_{sm} \tag{29}$$

$$E_{ss} = \begin{cases} E_s, \theta_{ss} < \theta_{baf} \\ K_{opt} \cdot K_{baf} \cdot E_s, \theta_{baf} \le \theta_{ss} < 90° \\ 0, 90° \le \theta_{ss} \end{cases} \tag{30}$$

$$E_{se} = \begin{cases} 0.35E_s, \theta_{se} < \theta_{baf} \\ 0.35K_{opt} \cdot K_{baf} \cdot E_s, \theta_{baf} \le \theta_{se} < 90° \\ 0, 90° \le \theta_{se} \end{cases} \tag{31}$$

$$E_{sm} = \begin{cases} E_m, \theta_{sm} < \theta_{baf} \\ K_{opt} \cdot K_{baf} \cdot E_m, \theta_{baf} \le \theta_{sm} < 90° \\ 0, 90° \le \theta_{sm} \end{cases} \tag{32}$$

where E_{stray} is the irradiancy of the stray at star sensor working height; E_s is the irradiancy of the sun at the star sensor working height, which could be obtained by Eq. (5); E_m is the irradiancy of the moon at the star sensor working height, which could be considered as E_m = 0.001 4 W/m^2 approximatively; E_e is the irradiancy of the EAR at the star sensor working height, which could be calculated by Eq. (9); θ_{baf} is the shielded angle of the baffle; K_{baf} is the extinction ratio of the baffle; K_{opt} is the extinction ratio of the optical lenses; θ_{ss} is the included angle between the star sensor optical axis point and the sunlight at any moment, which could be got by Eq. (18); θ_{sm} is the included angle between the star sensor optical axis point and the moonlight at any moment, which could be got by Eq. (26); θ_{se} is the included angle between the star sensor optical axis point and the EAR at any moment, which could be got by Eq. (28).

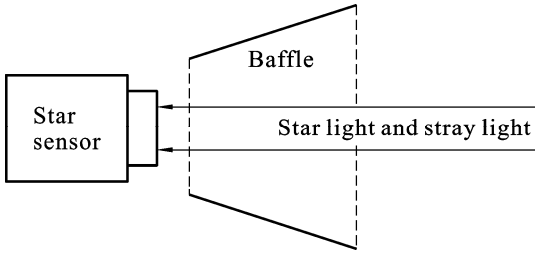

Fig. 4 Installation positions of star sensor and baffle

3 Space luminous environment adaptability

When the detection rate and the false alarm rate were given, the signal-noise rate (SNR) criterion to realize the optimal detection was

$$K = \frac{S}{N} \ge V_{th} \tag{33}$$

where K is SNR; S is the target signal; N is the root mean square value of noise signals; V_{th} is the SNR threshold. When the detection rate is more than 99% and the false alarm rate is less than 1%, the calculated V_{th} is 5 [22].

For a star sensor, SNR criterion should also be satisfied to realize the effective detection to star point targets. As an example, a star sensor with detection sensitivity of 6 apparent magnitude star in static state was considered. The irradiancy ratio (6 magnitude star to the stray) on the star sensor sensitization surface could be regarded as SNR.

$$K = \frac{E_{s6}}{E_{stray}} \tag{34}$$

where E_{stray} is the irradiancy of stray on the star sensor sensitization surface, which could be calculated by Eq. (32). E_{s6} is the irradiancy of 6 magnitude star on the star sensor sensitization surface, which could be expressed as

$$E_{s6} = \frac{E_{V6} \cdot \tau_{opt} \cdot D^2}{d_s^2} \tag{35}$$

where E_{V6} is the irradiancy of 6 magnitude star in exoatmosphere; τ_{opt} is the transmittance of the star sensor optical system; D is the clear aperture of the star sensor optical system; d_s is the diffuse spot radius of the star point target.

To make the stray have no effect on identifying 6 magnitude star, SNR expressed by Eq. (34) should satisfy

$$K = \frac{E_{s6}}{E_{stray}} > 5 \tag{36}$$

4 Simulation and analysis

The key calculating the included angle between the star sensor optical axis point and the stray (including the sunlight and the moonlight) was how to get the apparent position according to the analysis above. To verify the correctness of the apparent position calculation, the apparent position could be looked up in Stellarium and then could be compared with the calculation results of this work. Stellarium was a kind of virtual planetarium software [23]. According to the time and location of the observers, the position of the sun, the moon, planets and stars could be calculated and shown by Stellarium. The constellation could also be mapped and the astronomical phenomena (meteor shower, solar eclipse, lunar eclipse, etc) could be simulated by Stellarium. 99% of star data in the star catalog was from NOMAD (the first edition of the celestial body measurement data set organized by the US Naval Observatory), and the material of the common brighter stars was from Tycho2 star catalog and Hipparcos star catalog.

The sun apparent right ascension and the sun apparent declination on March 21, 2011 (the Spring Equinox) in Beijing (the latitude is 39°55′ N and the longitude is 116°24′ E) calculated by this work were compared with the results given by Stellarium. As shown in Fig. 5, the maximum error of the sun apparent right ascension was 0.012 6° and the maximum error of sun apparent declination was 0.002 7°. The moon apparent right ascension and the moon apparent declination calculated by this work were compared with the results given by Stellarium. As shown in Fig. 6, the maximum error of the moon apparent right ascension was 0.802 2° and the maximum error of moon apparent declination was 0.786 2°.

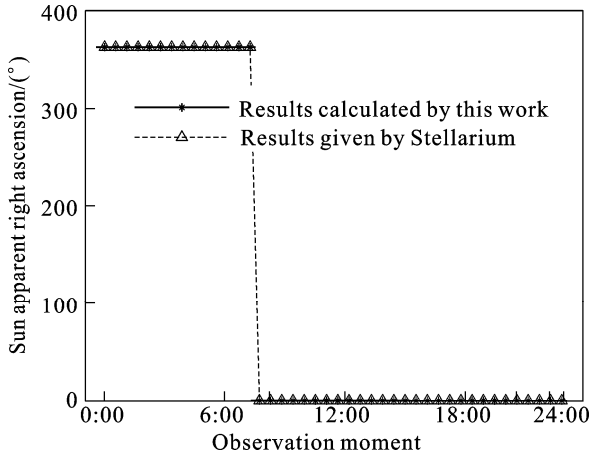

Fig. 5 Compare sun apparent right ascension and apparent declination calculated by this work with results given by Stellarium(Beijing time on March 21, 2011)

In consideration of March 21 (the Spring Equinox), July 22 (the Summer Solstice), September 23 (the Autumnal Equinox) and December 22 (the Winter Solstice) in 2011 in Beijing, the included angles between the star sensor optical axis point and the sunlight were shown in Fig. 7. It could be perceived that the included angles between the star sensor optical axis point and the sunlight were in accordance with the matter of fact. As an illustration, the included angle between star sensor optical axis point and the sunlight was the minimum on the Summer Solstice midday. At that moment, the sun shot the Tropic of Cancer and the height of the sun height reached the maximum. The star sensor optical axis was vertical and pointed to the sky when imaging, then the included angle between star sensor optical axis point and the sunlight should be the minimum. In consideration of August 29 (August 1 of the lunar year, new moon), September 5 (August 8 of the lunar year, first quarter moon), September 12 (August 15 of the lunar year, full moon) and September 20 (August 23 of the lunar year, last quarter moon) in 2011 in Beijing, the included angles between the star sensor optical axis point and the moonlight were shown in Fig. 8.

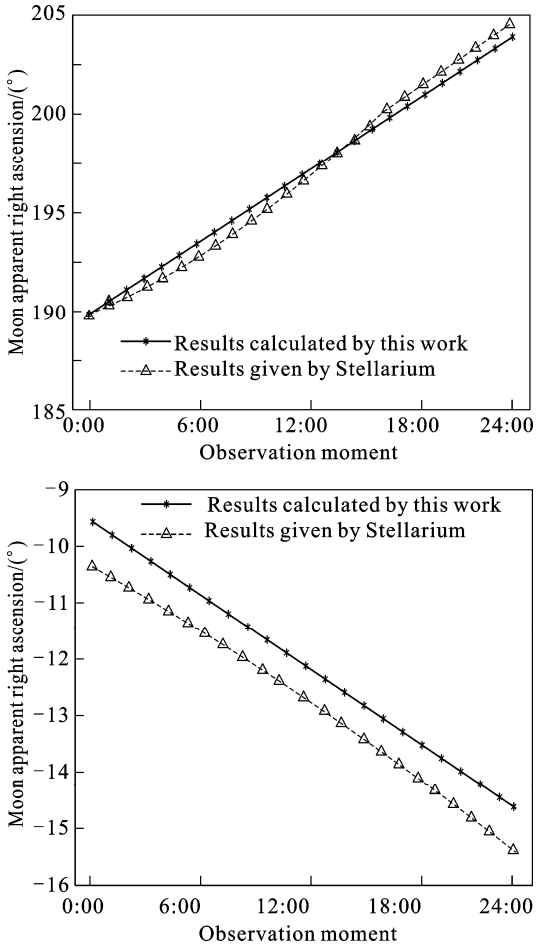

Fig. 6 Comparison of moon apparent right ascension and apparent declination calculated by this work with results given by Stellarium (Beijing time on March 21, 2011)

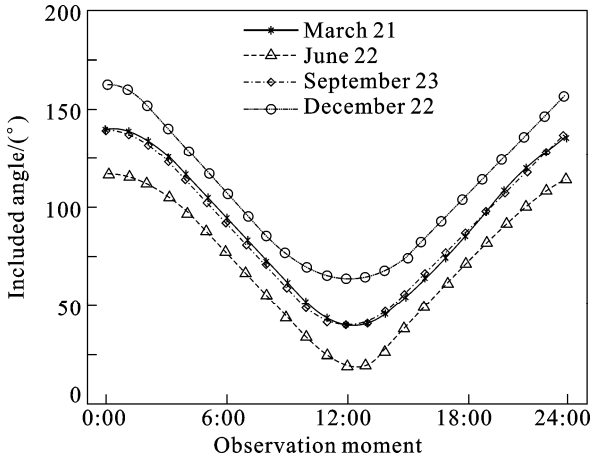

Fig. 7 Included angle between star sensor optical axis point and sunlight

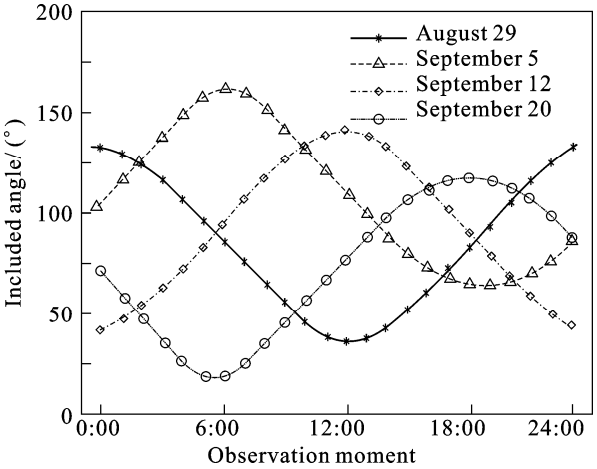

Fig. 8 Included angle between star sensor optical axis point and moonlight

Taking illustration as an example [24], the extinction ratio of the baffle was K_{baf} = 4.576×10^{-9}, the extinction ratio of the optical lenses was K_{opt}=0.1, and the shielded angle was θ_{baf}= 35°. The irradiancy of 6 magnitude star on the star sensor sensitization surface could be calculated by Eq. (35) as E_{6s}=2.63×10^{-5} W/m^2 [25]. If the star sensor optical axis was vertical and pointed to the sky while imaging, the space luminous environment star sensor imaging the starry sky on June 22, 2011 (the Summer Solstice) and September 20, 2011 (August 23 of the lunar year, last quarter moon) in Beijing could be obtained by Eq. (29) −Eq. (32). The results were shown in Fig. 9 and Fig. 10, respectively. Combined with Fig. 7, it could be known from Fig. 9 that: 1) During 0:00−4:00, the included angle between the star sensor optical axis point and the moonlight was 35°<θ_{sm}<90°. The moonlight was restrained by the baffle. The irradiancy of the stray at star sensor optical lenses was 4.72×10^{-13} W/m^2. The irradiancy of 6 magnitude star was E_{6s}=2.63×10^{-5} W/m^2 according to the reference. So the ratio of K described by Eq. (36) was far more than 5. There was no effect on the star point target identification. 2) During 5:00−9:00 and 15:00−19:00, the included angle between the star sensor optical axis point and the sunlight was 35°<θ_{ss}<90°. The sunlight was restrained by the baffle. The irradiancy of the stray at star sensor optical lenses was 3.9×10^{-7} W/m^2. K was much more than 5. There was no effect on the star point target identification. 3) During 10:00−14:00, the included angle between the star sensor optical axis point and the sunlight was θ_{ss}<35°. The sunlight entered into the star sensor FOV. The irradiancy of the stray at star sensor optical lenses was 858.5 W/m^2. K was far less than 5. The star point target was submerged by the stray. Combined with Fig. 8, it could be known from Fig. 10 that: 1) During 0:00–3:00 and at 23:00, the included angle between the star sensor optical axis point and the moonlight was 35°<θ_{sm}<90°. The moonlight was restrained by the baffle. The irradiancy of the stray at star sensor optical lenses was 4.72×10^{-13}W/m^2. K was far less than 5. There was no effect on the star point target identification. 2) During 4:00−8:00, the included angle between the star sensor optical axis point and the moonlight was θ_{sm} <35°. The moonlight entered into the star sensor FOV. The irradiancy of the stray at star sensor optical lenses was 0.001 4 W/m^2. K was far less than 5. The star point target was submerged by the stray. 3) During 9:00−18:00, the included angle between the star sensor optical axis point and the sunlight was 35°<θ_{ss}<90°. The sunlight was restrained by the baffle. The irradiancy of the stray at star sensor optical lenses was 4.1×10^{-7} W/m^2. K was much more than 5. There was no effect on the star point target identification. Therefore, when star sensors imaged the starry sky, an appropriate imaging time, a navigation star with certain orientation, a baffle with a high extinction ratio should be chosen. Then the stray interference could be avoided when the star sensor imaged the star in the sky.

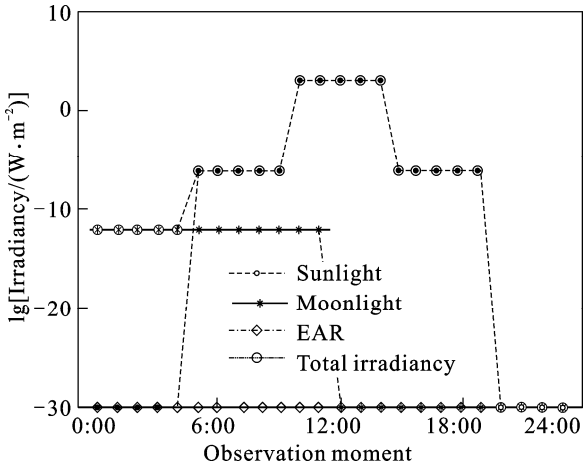

Fig. 9 Space luminous environment of star sensor on Summer Solstice

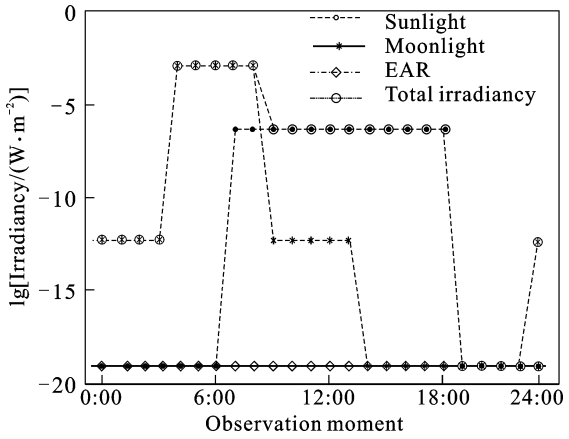

Fig. 10 Space luminous environment of star sensor on September 20, 2011

5 Conclusions

1) Irradiancy of the sunlight, the moonlight and the EAR at the missile-borne star sensor working height are estimated. The included angles between the star sensor optical axis point and the sunlight, the moonlight, the EAR are calculated. The calculating correctness of the sun apparent position and the moon apparent position is verified by the star image software of Stellarium. A real-time model for space luminous environment of missile-borne star sensor is proposed. The space luminous environment adaptability of missile-borne star sensor is analyzed.

2) When a certain type of star sensor images the starry sky on June 22, 2011 (the Summer Solstice) and September 20, 2011 (August 23rd in lunar calendar, last quarter moon) in Beijing, the space luminous environments are described by this model. The adaptability of the star sensor to space luminous environment is analyzed in period of time. The simulation results are identical with the actual situation. Based on determining the relative star sensor indexes (the shielded angle of baffle and the extinction ratio of baffle), the star chosen strategy and the missile launch window can then be provided.

References

[1] LIU Chao-shan, LIU Guang-bin, WANG Xin-guo, LI Ai-hua. The principle and system application of missile-borne star sensor [M]. Beijing: National Defense Industry Press, 2010: 35−37. (in Chinese)

[2] HU Hai-dong, HUANG Xian-lin, LI Ming-ming, SONG Zhuo-yue. Federated unscented particle filtering algorithm for SINS/CNS/GPS system [J]. Journal of Central South University of Technology, 2010, 17: 778–785.

[3] KAWANO H, SHIMOJI H, YOSHIKAWA S, MIYATAKE, HAMAK, NAKAMURAS. Suppression of sun interference in the star sensor baffling stray light by total internal reflection[J]. SPIE, 2005, 5962(1): 59621R.

[4] MA Jie. The study of circumstance adaptability of space camera [D]. Changchun: Changchun University of Science and Technology, 2009. (in Chinese)

[5] RUFINO G, ACCARDO D. Enhancement of the centroiding algorithm for star tracker measure refinement [J]. Acta Astronautica, 2003, 53: 135–147.

[6] LIEBE C C. Accuracy performance of star trackers- a tutorial [J]. IEEE Transactions on Aerospace and Electronic Systems, 2002, 38(2): 587–589.

[7] GRIFFITH D T, SINGLA P, JUNKINS J L. Autonomous on-orbit calibration approaches for star tracker cameras [J]. Astronautical Sciences, 2002, 112: 39–57.

[8] GUEYMARD C A. The Sun's total and spectral irradiance for solar energy applications and solar radiation models [J]. Solar Energy, 2004, 76(4): 423–453.

[9] ALMOROX J, HONTORIA C. Global solar radiation estimation using sunshine duration in Spain [J]. Energy Conversion and Management, 2004, 45(9/10): 1529–1535.

[10] WONG L T, CHOW W K. Solar radiation model [J]. Applied Energy, 2001, 69(3): 191–224.

[11] LI Shu-jun, GAO Xiao-dong, ZHU Qi-xiang. Analysis for luminosity features of a satellite with solar battery panels [J]. Opto-Electronic Engineering, 2004, 31(4):1–8. (in Chinese).

[12] MEEUS J. Astronomical algorithms[M]. Virginia, USA: Willmann-Bell Inc, 1998: 307–315.

[13] MONTENBRUCK O，PFLEGER T. Astronomy on the personal computer [M]. Heidelberg: Springer Verlag, 2000: 35–40.

[14] YANG Chun-ping, MENG Xue-qing, WU Jian. Approximate model for calculating radiance of atmospheric background [C]//The 4th International Symposium on Advanced Optical Manufacturing and Testing, Bellingham: SPIE, 2009, 7283(3s): 1–5.

[15] GUO Q, XU J M, ZHANG W J. Stray light modeling and analysis for the FY-2 meteorological satellite [J]. International Journal of Remote Sensing, 2005, 26(13): 2817–2830.

[16] YUAN Yu-kai, CHEN Hong-yu, WU Hui-ying. In-orbit spacecraft's earth and atmosphere radiation environment analysis [J]. Journal of Beijing University of Aeronautics and Astronautics, 2011, 37(2): 136–139. (in Chinese).

[17] ZHANG Wei, WANG Hong-yuan, WANG Zhi-le. Modeling method for visible scattering properties of space target [J]. Acta Photonica Sinica, 2008, 37(12): 2462–2467. (in Chinese).

[18] XU Gen-xing. Optical characteristic of the object and environment [M]. Beijing: Astronavigation Press, 1995: 213–223. (in Chinese).

[19] REDA I, ANDREAS A. Solar position algorithm for solar radiation applications [J]. Solar Energy, 2004, 76(5): 577–589.

[20] GRENA R. An algorithm for the computation of the solar position [J]. Solar Energy, 2008, 82(5): 462–470.

[21] CHANG T P. The Sun's apparent position and the optimal tilt angle of a solar collector in the northern hemisphere [J]. Solar Energy, 2009, 83(8): 1274–1284.

[22] ZHANG Chen, CHEN Chao-yang, SHEN Xu-bang. Study on detection sensitivity of an APS star tracker. [J]. Opto-Electronic Engineering, 2004, 31(10): 17–20.

[23] HUGHES S. Stellarium– A valuable resource for teaching astronomy in the classroom and beyond [J]. Science Education News, 2008, 57(2): 83–86.

[24] LIAO Zhi-bo, FU Rui-min, ZONG Xiao-ying. Optimal designing of baffle of star sensor [J]. Chinese Journal of Lasers, 2010, 37(4): 987–990. (in Chinese).

[25] FENG Guang-jun, MA Zhen, LI Ying-cai. Design and performance analysis of standard starlight simulator [J]. Journal of Applied Optics, 2010, 31(1): 39–42. (in Chinese).

(Edited by HE Yun-bin)